

**Cross-polarization mode coupling and exceptional points in photonic crystal slabs**

Dmitry A. Bykov\* and Leonid L. Doskolovich

*Image Processing Systems Institute—Branch of the Federal Scientific Research Centre “Crystallography and Photonics” of Russian Academy of Sciences, 151 Molodogvardeyskaya Street, Samara 443001, Russia  
and Samara National Research University, 34 Moskovskoye Shosse, Samara 443086, Russia*

(Received 7 November 2017; published 26 January 2018)

We study exceptional points that occur in photonic crystal slabs due to cross-polarization (TE-TM) mode coupling. To do this, we develop spatiotemporal coupled-mode theory that describes optical properties of photonic crystal slabs supporting TE and TM modes in the case of conical mount. The developed theory suggests that by tuning the in-plane wave numbers of the incident light one can make two modes of the structure coalesce, which results in an exceptional point. The developed theory provides simple analytical expressions for the exceptional point position and the line shape of the corresponding resonance. The parameters of the proposed model can be rigorously estimated by a numerical calculation of the S-matrix poles of the structure. We show that the proposed analytical model with the estimated parameters is in good agreement with the presented full-wave simulations.

DOI: [10.1103/PhysRevA.97.013846](https://doi.org/10.1103/PhysRevA.97.013846)**I. INTRODUCTION**

In recent years much attention has been paid to studying exceptional points in optical structures [1–6]. Exceptional points (EPs) occur when both eigenfrequencies and field distributions of several modes of the structure coincide [7–9]. Exceptional points of order 2 can be obtained by tuning two real-valued parameters of the structure. The tuning of  $N$  independent parameters allows one to make  $N$  eigenmodes of the structure coalesce, which results in an EP of order  $N$  [5,10,11].

Exceptional points are studied in different branches of physics, including acoustics [12], atomic physics [13,14], and optics. In optics, various structures with EP behavior were investigated, such as photonic crystal slabs [2], parallel waveguides [10,11], optical cavities [5], metamaterials [15], and different plasmonic [16,17] and graphene-based [18] optical structures. Particular attention was paid to studying  $\mathcal{PT}$ -symmetric structures [1,5,11,19].

Structures with EPs exhibit intriguing optical effects such as non-Lorentzian (and non-Fano) resonance line shape [9,20], loss-induced transparency [1], and asymmetric light reflection and transmission [4,17,19,21]. Other applications of EP structures include controlling light emission [3,22] and optical sensing [5,6,23].

As a rule, exceptional points are studied through analyzing the eigenvalues and eigenvectors of the Hamiltonian [8,9]. In Ref. [2] an *effective* Hamiltonian was used to write down the temporal coupled-mode theory (CMT) describing EPs in photonic crystal slabs [2]. Similar CMT was used to describe coupled optical cavities in Ref. [5].

In this paper, we use the recently proposed spatiotemporal coupled-mode theory [24,25] to study EPs in one-dimensional (1D) photonic crystal slabs (PCSs) [see Fig. 1(a)]. In the case of planar diffraction, a PCS supports TE and TM

modes, which are uncoupled. However, in the case of conical diffraction, polarization transformation occurs, which makes cross-polarization mode excitation possible [25]. In this paper, we study a similar effect—cross-polarization mode *coupling*. This effect, as we show, can be described using the proposed spatiotemporal coupled-mode theory. Additionally, this theory predicts the emergence of an exceptional point in the considered structure. Comparing to Refs. [2,5] the proposed model gives simple interpretation of the parameters of the CMT. Moreover, we show that these parameters can be rigorously calculated by finding the poles of the scattering matrix of the structure.

The paper is organized in five sections. The Introduction is followed by Sec. II that presents the spatiotemporal coupled-mode theory of cross-polarization mode coupling in a 1D PCS. In Sec. III we show that the considered structure supports exceptional points and derive analytical estimations for the EP conditions. In Sec. IV we calculate the parameters of the proposed model and compare the CMT-based predictions with full-wave simulations based on the rigorous coupled-wave analysis. Section V concludes the paper.

**II. SPATIOTEMPORAL COUPLED-MODE THEORY**

Let us consider the diffraction of a TM-polarized plane wave by a 1D photonic crystal slab shown in Fig. 1(a). The direction of the incident wave is defined by the in-plane wave-vector components,  $k_x$  and  $k_y$ . In the case of planar diffraction ( $k_y = 0$ ), the PCS supports TE and TM modes. The modes having the same polarization (TM-TM or TE-TE) can couple with each other, which results in the anticrossing of the dispersion curves. In the case of conical mount ( $k_y \neq 0$ ), the polarization transformation takes place: the modes contain both TE and TM field components. However, for small values of  $k_y$  the modes of the structure can still be referred to as (quasi-)TE and (quasi-)TM modes. The quasi-TE modes have strong TE components and “weak” TM components. Similarly, quasi-TM

\*bykovd@gmail.com

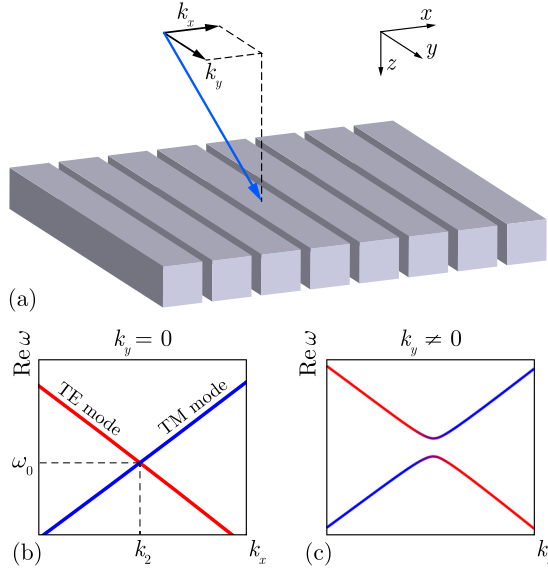


FIG. 1. (a) Geometry of a 1D PCS (parameters: period  $d = 1000$  nm; height  $h = 800$  nm; fill factor  $4/5$ ; surrounding medium refractive index  $n_s = 1$ ; structure material permittivity  $\epsilon_{gr} = 2$ ). The structure is invariant in the  $y$  direction. (b) Crossing of dispersion curves of TE and TM modes at  $k_y = 0$ . (c) Cross-polarization mode coupling at  $k_y \neq 0$ .

modes have dominant TM components. Due to polarization conversion, TE-TM coupling can occur in the case of conical mount. In this section we develop a coupled-mode theory which describes this effect.

Following the approach used in Refs. [24,25], we start our analysis by considering not the modes of the PCS but the modes of a slab waveguide with an effective refractive index. We will assume that the waveguide supports TE- and TM-polarized modes. Let us further assume that the TM mode has the group velocity  $v_g^{\text{TM}}$  at the angular frequency  $\omega_0$ . In this case, we can write the following approximate dispersion law of the mode:

$$k - k^{\text{TM}} = (\omega - \omega_0)/v_g^{\text{TM}}, \quad (1)$$

where  $k$  and  $k^{\text{TM}}$  are the wave numbers of the mode at angular frequencies  $\omega$  and  $\omega_0$ , respectively. We will assume that

$v_g^{\text{TM}} > 0$ , so the mode propagates in the positive  $x$  direction. Similarly, we define the dispersion law of the counterpropagating TE mode as

$$k + k^{\text{TE}} = -(\omega - \omega_0)/v_g^{\text{TE}}. \quad (2)$$

If  $d$  is the period of the PCS, the diffraction orders have the following  $x$  components of the wave vector:  $k_x + mk_1$ , where  $k_1 = 2\pi/d$  and  $m \in \mathbb{Z}$ . We will assume that  $k_{\text{TM}} = k_2 + k_1$ , so the TM mode can be excited by the +1st diffraction order when the incident light has angular frequency  $\omega_0$  and  $x$  component of the wave vector  $k_2$ . We will further assume that  $-k_{\text{TE}} = k_2 - k_1$ ; hence the TE-polarized mode can be excited by the -1st diffraction order at  $\omega = \omega_0, k_x = k_2, k_y = 0$ . These assumptions describe the crossing of the dispersion curves of the TE and TM modes, as shown in Fig. 1(b).

The dispersion curves (1) and (2) intersect at the point  $(k_2, \omega_0)$ . In what follows, we develop coupled-mode theory that is valid in the vicinity of this point. We will further assume that  $k_2 \neq 0$ , so the intersection of the TE and TM dispersion curves will take place not in the center of the first Brillouin zone. In this case, we can neglect the TM mode that propagates in the negative  $x$  direction and the TE mode propagating in the positive  $x$  direction.

To develop the coupled-mode theory let us first write two paraxial unidirectional wave equations, which describe the propagation of the modal wave packets inside the waveguide [25]:

$$\begin{aligned} \frac{\partial u}{\partial t} &= -v_g^{\text{TM}} \frac{\partial u}{\partial x} + \frac{iv_g^{\text{TM}}}{2k^{\text{TM}}} \frac{\partial^2 u}{\partial y^2} + i(v_g^{\text{TM}} k^{\text{TM}} - \omega_0)u, \\ \frac{\partial v}{\partial t} &= v_g^{\text{TE}} \frac{\partial v}{\partial x} + \frac{iv_g^{\text{TE}}}{2k^{\text{TE}}} \frac{\partial^2 v}{\partial y^2} + i(v_g^{\text{TE}} k^{\text{TE}} - \omega_0)v. \end{aligned} \quad (3)$$

Here  $u(x, y, t)$  and  $v(x, y, t)$  are the complex amplitudes of the TM and TE modes, respectively. By introducing the coupling terms in the right-hand side of Eqs. (3), we obtain the following set of coupled-mode equations, which describe light diffraction by the periodically perforated slab waveguide that is the PCS [24,25]:

$$\begin{cases} \frac{\partial u}{\partial t} = -v_g^{\text{TM}} \frac{\partial u}{\partial x} + \frac{iv_g^{\text{TM}}}{2k^{\text{TM}}} \frac{\partial^2 u}{\partial y^2} + i(v_g^{\text{TM}} k^{\text{TM}} - \omega_0)u - c_1^{\text{TM}} u + \hat{\mathbf{c}}_2^{\text{TM}} e^{2ik_1 x} v + c_e^{\text{TM}} e^{ik_1 x} f_I, \\ \frac{\partial v}{\partial t} = v_g^{\text{TE}} \frac{\partial v}{\partial x} + \frac{iv_g^{\text{TE}}}{2k^{\text{TE}}} \frac{\partial^2 v}{\partial y^2} + i(v_g^{\text{TE}} k^{\text{TE}} - \omega_0)v - c_1^{\text{TE}} v + \hat{\mathbf{c}}_2^{\text{TE}} e^{-2ik_1 x} u + \hat{\mathbf{c}}_e^{\text{TE}} e^{-ik_1 x} f_I, \\ f_T = t_0 f_I + c_t^{\text{TM}} e^{-ik_1 x} u + \hat{\mathbf{c}}_t^{\text{TE}} e^{ik_1 x} v. \end{cases} \quad (4)$$

Here  $f_I = f_I(x, y, t)$  is the incident field distribution, and  $f_T = f_T(x, y, t)$  is the TM-polarized transmitted field. The transmitted field is the sum of the light leaked out of the PCS and the nonresonantly transmitted light, which is defined by the nonresonant transmission coefficient  $t_0$  [24]. The exponentials in Eq. (4) take account of the phase change due to scattering

into the diffraction order [24,26]. The coupling coefficients  $c_1^{\text{TM}}$  and  $c_1^{\text{TE}}$ , which are real numbers, describe the leakage of the mode out of the waveguide. The terms  $\hat{\mathbf{c}}_2^{\text{TM}}$  and  $\hat{\mathbf{c}}_2^{\text{TE}}$  describe coupling between the TM and TE modes;  $c_e^{\text{TM}}$  and  $\hat{\mathbf{c}}_e^{\text{TE}}$  describe excitation efficiency of the modes by the incident TM-polarized plane wave;  $c_t^{\text{TM}}$  and  $\hat{\mathbf{c}}_t^{\text{TE}}$  describe light outcoupling

from the modes to the considered TM-polarized transmitted diffraction order. The coupling coefficients typeset as bold letters with a hat describe cross-polarization scattering. Reference [25] suggests that these coefficients should be treated as linear operators with the form defined by the symmetry of the structure.

Coupled-mode equations (4) can be solved in the Fourier domain. To do this, we define the Fourier transform as

$$\mathcal{F}u = \iiint_{\mathbb{R}^3} u(x, y, t) e^{-i(k_x x + k_y y - \omega t)} dk_x dk_y d\omega \quad (5)$$

and introduce the following notations:  $F_I = \mathcal{F}f_I$  is the spectrum of the incident field,  $F_T = \mathcal{F}f_T$  is the spectrum of the

transmitted field, and  $U = \mathcal{F}(u e^{-ik_1 x})$  and  $V = \mathcal{F}(v e^{ik_1 x})$  are the envelope spectra of the modes  $u$  and  $v$ .

In Ref. [25] it was shown that in the Fourier domain the coupling operators used in Eq. (4) become coupling coefficients that depend on  $k_y$ . For example, the coupling operator  $\hat{\mathbf{c}}_e^{\text{TE}}$  takes the following form:

$$\mathcal{F}(\hat{\mathbf{c}}_e^{\text{TE}} f) = k_y c_e^{\text{TE}} \mathcal{F}f, \quad (6)$$

where  $c_e^{\text{TE}}$  is a number. We will use similar relations for operators  $\hat{\mathbf{c}}_t^{\text{TE}}$ ,  $\hat{\mathbf{c}}_2^{\text{TM}}$ , and  $\hat{\mathbf{c}}_2^{\text{TE}}$ .

By applying the Fourier transform (5) to the coupled-mode equations (4), we obtain the following system:

$$\begin{cases} -i\omega U = -iv_g^{\text{TM}}(k_x - k_2)U - i\eta^{\text{TM}}k_y^2 U - (i\omega_0 + c_1^{\text{TM}})U + c_2^{\text{TM}}k_y V + c_e^{\text{TM}}F_I, \\ -i\omega V = iv_g^{\text{TE}}(k_x - k_2)V - i\eta^{\text{TE}}k_y^2 V - (i\omega_0 + c_1^{\text{TE}})V + c_2^{\text{TE}}k_y U + c_e^{\text{TE}}k_y F_I, \\ F_T = t_0 F_I + c_t^{\text{TM}}U + c_t^{\text{TE}}k_y V, \end{cases} \quad (7)$$

where  $\eta^{\text{TM}} = \frac{v_g^{\text{TM}}}{2k^{\text{TM}}}$ ,  $\eta^{\text{TE}} = \frac{v_g^{\text{TE}}}{2k^{\text{TE}}}$ . The complex transmission coefficient of the PCS can be obtained from Eq. (7) as the ratio of the transmitted and incident field spectra:  $T = F_T/F_I$  [24,25].

System (7) can be written in the following matrix form:

$$\begin{cases} \mathbf{A} \begin{bmatrix} U \\ V \end{bmatrix} = i \begin{bmatrix} c_e^{\text{TM}} \\ c_e^{\text{TE}} k_y \end{bmatrix} F_I, \\ F_T = t_0 F_I + \begin{bmatrix} c_t^{\text{TM}} & c_t^{\text{TE}} k_y \end{bmatrix} \begin{bmatrix} U \\ V \end{bmatrix}, \end{cases} \quad (8)$$

where

$$\mathbf{A} = \begin{bmatrix} \omega - \omega_0 + ic_1^{\text{TM}} - v_g^{\text{TM}}(k_x - k_2) - \eta^{\text{TM}}k_y^2 & -ic_2^{\text{TM}}k_y \\ -ic_2^{\text{TE}}k_y & \omega - \omega_0 + ic_1^{\text{TE}} + v_g^{\text{TE}}(k_x - k_2) - \eta^{\text{TE}}k_y^2 \end{bmatrix}. \quad (9)$$

By inverting the matrix  $\mathbf{A}$ , one can solve Eq. (8) for the complex transmission coefficient  $T = F_T/F_I$ :

$$T = t_0 + \frac{q}{\det \mathbf{A}}. \quad (10)$$

The expression for the numerator  $q$  has a complicated form and is not presented here, while the denominator is easily expressed as

$$\begin{aligned} \det \mathbf{A} &= [\omega - \omega_0 + ic_1^{\text{TM}} - v_g^{\text{TM}}(k_x - k_2) - \eta^{\text{TM}}k_y^2] \\ &\quad \times [\omega - \omega_0 + ic_1^{\text{TE}} + v_g^{\text{TE}}(k_x - k_2) - \eta^{\text{TE}}k_y^2] \\ &\quad + c_2^2 k_y^2, \end{aligned} \quad (11)$$

where

$$c_2 = \sqrt{c_2^{\text{TM}} c_2^{\text{TE}}}.$$

By equating the determinant (11) to zero, we obtain the dispersion equation of the modes of the structure:

$$\det \mathbf{A} = 0. \quad (12)$$

Indeed, when Eq. (12) holds, the solution to coupled-mode equations (8) exists in the absence of the incident field (at  $F_I = 0$ ).

At  $k_y = 0$ , the dispersion equation (12) describes two intersecting lines, which correspond to the TE and TM modes [see Fig. 1(b)]. In the case of conical diffraction mount,  $k_y$  is nonzero, and the two modes couple, which, starting from some value of  $k_y$ , results in the formation of a band gap, as it is shown in Fig. 1(c). This effect can be called cross-polarization mode coupling. In the next section we will consider the special case separating the crossing of dispersion curves shown in Fig. 1(b) from the anticrossing behavior shown in Fig. 1(c).

### III. EXCEPTIONAL POINT

The dispersion equation (12) is a quadratic equation with respect to  $\omega$ , and it has two roots. It is easy to verify that these two roots coincide if the following equality holds:

$$\begin{aligned} (c_1^{\text{TE}} - c_1^{\text{TM}}) - i(k_x - k_2)(v_g^{\text{TM}} + v_g^{\text{TE}}) \\ = i[(\eta^{\text{TM}} - \eta^{\text{TE}})k_y^2 \pm 2c_2 k_y]. \end{aligned} \quad (13)$$

Equation (13) describes the borderline case between dispersion of Figs. 1(b) and 1(c).

One can choose real values of  $k_x$  and  $k_y$  to satisfy Eq. (13). Indeed, by assuming that  $\eta$  and  $v_g$  are real numbers, we equate

the real and imaginary parts of the left- and right-hand sides of Eq. (13) and obtain the following values of  $k_y$  and  $k_x$ :

$$\tilde{k}_y = \pm \frac{c_1^{\text{TM}} - c_1^{\text{TE}}}{2 \text{Im } c_2}, \quad (14)$$

$$\tilde{k}_x = k_2 - \frac{\tilde{k}_y^2 (\eta^{\text{TM}} - \eta^{\text{TE}}) + 2|\tilde{k}_y| \text{Re } c_2}{v_g^{\text{TM}} + v_g^{\text{TE}}}. \quad (15)$$

If we choose the direction of the incident wave according to Eqs. (14) and (15), the complex frequencies of the two modes of the structure coincide. This, as we will prove further, results in an emergence of the so-called exceptional point.

According to Eq. (14), the higher the difference between the extinction rates of the TE and TM modes of the structure, the higher the value of  $\tilde{k}_y$  that should be used to obtain an exceptional point. Besides, according to Eq. (15), the value of  $\tilde{k}_x$ , which allows us to obtain an exceptional point, is generally different from the value of  $k_2$ , which gives the intersection point of the dispersion curves of the TM- and TE-polarized modes at  $k_y = 0$  [see Fig. 1(b)].

Taking into account Eqs. (14) and (15), we can solve Eq. (12) for  $\omega = \omega_p$  to obtain the value of the complex frequency of the structure eigenmode:

$$\omega_p = \omega_0 - i \frac{c_1^{\text{TM}} + c_1^{\text{TE}}}{2} + \frac{v_g^{\text{TM}} - v_g^{\text{TE}}}{2} (\tilde{k}_x - k_2) + \frac{\eta^{\text{TM}} + \eta^{\text{TE}}}{2} \tilde{k}_y^2. \quad (16)$$

Equations (14)–(16) allow us to rewrite Eq. (10) in the following form:

$$T = t_0 + \frac{a}{\omega - \omega_p} + \frac{b}{(\omega - \omega_p)^2}. \quad (17)$$

Here  $a$  and  $b$  depend on the coupling coefficients; however, the closed-form expressions for  $a$  and  $b$  are quite complicated and are not presented in this paper. Nevertheless, we can infer that the first two terms in Eq. (17) correspond to simple Fano line shape, while the third term contains a second-order pole, which is the evidence of an exceptional point [9,20].

Equation (17) can be rewritten in the following elegant form, which immediately follows from Eq. (8):

$$T = t_0 + i [c_t^{\text{TM}} \quad \tilde{k}_y c_t^{\text{TE}}] (\mathbf{I} \omega - \mathbf{\Omega})^{-1} \begin{bmatrix} c_e^{\text{TM}} \\ \tilde{k}_y c_e^{\text{TE}} \end{bmatrix}, \quad (18)$$

where  $\mathbf{I}$  is a  $2 \times 2$  identity matrix and

$$\mathbf{\Omega} = \begin{bmatrix} \omega_p - c_2 \tilde{k}_y & i c_2^{\text{TM}} \tilde{k}_y \\ i c_2^{\text{TE}} \tilde{k}_y & \omega_p + c_2 \tilde{k}_y \end{bmatrix}. \quad (19)$$

Note that since  $\hat{c}_t^{\text{TE}}$  is an operator the value of  $\tilde{k}_y c_t^{\text{TE}}$  can be interpreted as the coupling coefficient, which is calculated for the value of  $k_y = \tilde{k}_y$ .

The transmission coefficient  $T$  defined by Eq. (18) relates the complex amplitudes of one incident and one transmitted wave. In the framework of the coupled-mode theory one can consider several incident waves and several scattered diffraction orders. In this case, the right-hand sides of Eqs. (4) will contain several terms corresponding to the incident waves of different directions and polarizations. Additionally, for each

scattered diffraction order one should write a separate equation similar to the third equation of system (4). As the result, the coupled-mode theory gives the following form of the scattering matrix:

$$\mathbf{S} = \mathbf{S}_0 + \mathbf{B}(\mathbf{I}\omega - \mathbf{\Omega})^{-1} \mathbf{C}, \quad (20)$$

where  $\mathbf{S}_0$  is the nonresonant scattering matrix,  $\mathbf{C}$  is the incident-field-to-mode coupling matrix,  $\mathbf{B}$  is the mode-to-scattered-field coupling matrix, and  $\mathbf{\Omega}$  is defined by Eq. (19). Equation (20) is similar to the representation of the scattering matrix in the vicinity of resonances considered in Ref. [27]. The difference is that  $\mathbf{\Omega}$  is no longer a diagonal matrix. Moreover, it is nondiagonalizable: one can easily verify that the Jordan normal form of  $\mathbf{\Omega}$  contains a Jordan block of size  $2 \times 2$ , which is the evidence [28] of an exceptional point of order 2.

In this section we have shown that by choosing the direction of the incident light one can make the complex frequencies of the quasi-TE and quasi-TM modes coincide. This results in a distinguishable line shape of the resonance and in the emergence of an exceptional point.

#### IV. NUMERICAL VALIDATION

In this section, we compare CMT predictions with rigorous simulation results. As an example, we consider the 1D PCS shown in Fig. 1. The parameters of the structure are presented in the caption of Fig. 1. We will study the optical properties of this structure in the vicinity of  $k_x = 0.5 \mu\text{m}^{-1}$ ,  $k_y = 0$ , and  $\omega = 1.665 \times 10^{15} \text{ s}^{-1}$ . In Sec. IV A, we compare the dispersion curves of the eigenmodes; in Sec. IV B, we investigate the EP position and resonance line shape.

##### A. Mode dispersion comparison

To describe the dispersion of the modes within the CMT, we need to estimate the parameters used in Eq. (11). We will do this by calculating complex frequencies of the modes of the structure using the method of Ref. [27]. This method is based on finding the poles of the scattering matrix, which is calculated using the rigorous coupled-wave analysis [29,30]. The method of Ref. [27] allows us to calculate the mode frequency  $\omega_p(k_x, k_y)$  for the given in-plane wave numbers  $k_x$  and  $k_y$  and initial approximation of the mode frequency.

First, we calculate  $k_2$  and  $\omega_0$ , which define the intersection point of the dispersion curves of the TE and TM modes at  $k_y = 0$  [see Fig. 1(b)]. One can do this by solving the equation

$$\text{Re } \omega_p^{\text{TM}}(k_2, 0) = \text{Re } \omega_p^{\text{TE}}(k_2, 0) \quad (21)$$

for  $k_2$  using Newton's method. After calculating  $k_2$ , the value of  $\omega_0$  can be calculated as

$$\omega_0 = \text{Re } \omega_p^{\text{TM}}(k_2, 0) = \text{Re } \omega_p^{\text{TE}}(k_2, 0). \quad (22)$$

Additionally, according to Eqs. (11) and (12), the imaginary parts of the complex frequencies of the modes at  $k_x = k_2, k_y = 0$  give the values of  $c_1^{\text{TM}}$  and  $c_1^{\text{TE}}$ :

$$c_1^{\text{TM}} = -\text{Im } \omega_p^{\text{TM}}(k_2, 0), \quad c_1^{\text{TE}} = -\text{Im } \omega_p^{\text{TE}}(k_2, 0). \quad (23)$$

Second, the group velocities of the modes are easily calculated by numerical differentiation of the modes complex

frequencies with respect to  $k_x$ :

$$v_g^{\text{TM}} = \frac{\partial \omega_p^{\text{TM}}}{\partial k_x}(k_2, 0), \quad v_g^{\text{TE}} = \frac{\partial \omega_p^{\text{TE}}}{\partial k_x}(k_2, 0). \quad (24)$$

Third, to estimate  $\eta^{\text{TE}}$  and  $\eta^{\text{TM}}$ , we choose a wave number  $k_3$ , which is rather far from  $k_2$ . In this case, we can neglect the last term in Eq. (11), which brings us to the following estimations:

$$\eta^{\text{TE}} = \frac{1}{2} \frac{\partial^2 \omega_p^{\text{TE}}}{\partial k_y^2}(k_3, 0), \quad \eta^{\text{TM}} = \frac{1}{2} \frac{\partial^2 \omega_p^{\text{TM}}}{\partial k_y^2}(k_3, 0). \quad (25)$$

Finally, we differentiate Eq. (12) with respect to  $k_y$  twice, and, assuming  $k_x = k_2, k_y = 0, \omega = \omega_p^{\text{TE}}$ , we obtain the following expression for  $c_2$ :

$$c_2^2 = i \frac{c_1^{\text{TE}} - c_1^{\text{TM}}}{2} \left( \frac{\partial^2 \omega_p^{\text{TE}}}{\partial k_y^2}(k_2, 0) - 2\eta^{\text{TE}} \right). \quad (26)$$

For the considered structure, Eqs. (21)–(26) give the following parameters of the CMT:

$$\begin{aligned} \omega_0 &= 1.665830 \times 10^{15} \text{ s}^{-1}, \\ k_2 &= 0.47570 \mu\text{m}^{-1}, \\ c_1^{\text{TE}} &= 2.497 \times 10^{12} \text{ s}^{-1}, \\ c_1^{\text{TM}} &= 8.941 \times 10^{11} \text{ s}^{-1}, \\ v_g^{\text{TE}} &= 2.0260 \times 10^{17} \text{ nm/s}, \\ v_g^{\text{TM}} &= 1.9783 \times 10^{17} \text{ nm/s}, \\ \eta^{\text{TE}} &= 2.1995 \times 10^{19} \text{ nm}^2/\text{s}, \\ \eta^{\text{TM}} &= 1.5649 \times 10^{19} \text{ nm}^2/\text{s}, \\ c_2 &= 7.73 \times 10^{14} + 6.27 \times 10^{15}i \text{ nm/s}. \end{aligned} \quad (27)$$

We will use these parameters to calculate the dispersion of the modes of the structure using Eq. (12).

Figure 2 shows the dispersion curves of the modes of the structure. The red line (marked as ‘‘TE’’) shows the dispersion of TE-polarized mode at  $k_y = 0$ , while the TM-polarized mode is shown by the blue line (marked as ‘‘TM’’). Since

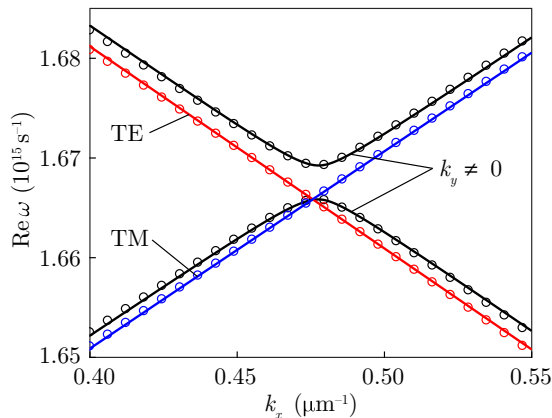


FIG. 2. Rigorously calculated dispersion curves of the PCS at  $k_y = 0$  and  $0.3 \mu\text{m}^{-1}$  (circles); dispersion curves are calculated using the CMT [Eqs. (11) and (12)] (solid lines).

no cross-polarization coupling occurs at  $k_y = 0$ , these lines cross. In the case of conical mount ( $k_y = 0.3 \mu\text{m}^{-1}$ , black line), cross-polarization coupling occurs, as it is evident from Fig. 2. The circles show the rigorously calculated dispersion curves, while the solid lines show the analytical approximation obtained using the CMT of Sec. II. Figure 2 suggests that the proposed model is in good agreement with the rigorous simulation results.

Let us discuss field distribution of the modes at different points of the dispersion curves. As we mentioned in the beginning of Sec. II, in the case of conical mount, modes have both TE and TM field components. The mode field calculations show that at  $k_x = 0.40 \mu\text{m}^{-1}, k_y = 0.3 \mu\text{m}^{-1}$  the (quasi-)TE modes have dominant TE components which are approximately ten times stronger than TM components. Similarly, (quasi-)TM modes have strong TM components and order-of-magnitude weaker TE components. However, when cross-polarization mode coupling occurs ( $k_x = 0.48 \mu\text{m}^{-1}, k_y = 0.3 \mu\text{m}^{-1}$ ) the TE and TM field components of the modes have equal strength.

### B. Exceptional point comparison

The exact position of the exceptional point in the considered structure can be obtained with the following Newton-like iterative approach. We start with some values of  $k_x$  and  $k_y$ . First, we calculate the complex frequencies of two modes,  $\omega_p^{\text{TE}}(k_x, k_y)$  and  $\omega_p^{\text{TM}}(k_x, k_y)$ , and their derivatives with respect to  $k_x$  and  $k_y$ . Second, we find a Newton approximation of the exceptional point,  $k'_x$  and  $k'_y$ , by equating the real and imaginary parts of the following linear equation:

$$\begin{aligned} \omega_p^{\text{TE}} + \frac{\partial \omega_p^{\text{TE}}}{\partial k_x} \times (k'_x - k_x) + \frac{\partial \omega_p^{\text{TE}}}{\partial k_y} \times (k'_y - k_y) \\ = \omega_p^{\text{TM}} + \frac{\partial \omega_p^{\text{TM}}}{\partial k_x} \times (k'_x - k_x) + \frac{\partial \omega_p^{\text{TM}}}{\partial k_y} \times (k'_y - k_y), \end{aligned} \quad (28)$$

where  $\omega_p^{\text{TE}}, \omega_p^{\text{TM}}$ , and the derivatives are calculated at the point  $(k_x, k_y)$ . The left-hand side of this equation is the Taylor series for  $\omega_p^{\text{TE}}(k_x, k_y)$ , while the right-hand side corresponds to  $\omega_p^{\text{TM}}(k_x, k_y)$ . Therefore, this equation is aimed at equating the complex frequencies of the two modes. Finally, we replace the EP approximation  $(k_x, k_y)$  with  $(\alpha k_x + (1 - \alpha)k'_x, \alpha k_y + (1 - \alpha)k'_y)$ , where  $\alpha = 8/9$  is a damping coefficient. To start the next iteration, we calculate the revised values of  $\omega_p^{\text{TE}}$  and  $\omega_p^{\text{TM}}$  using their previous values as the initial approximations. The damping coefficient  $\alpha$  reduces the convergence rate of the Newton method, ensuring that the previous values of  $\omega_p^{\text{TE}}$  and  $\omega_p^{\text{TM}}$  are good approximations for the consequent values of  $\omega_p^{\text{TE}}$  and  $\omega_p^{\text{TM}}$ , so the method of Ref. [27] converges to the desired mode.

The following parameters of the EP were obtained using the described approach:

$$\begin{aligned} k_x^{\text{EP}} &= 0.47647 \mu\text{m}^{-1}, \\ k_y^{\text{EP}} &= 0.12905 \mu\text{m}^{-1}, \\ \omega_{\text{EP}} &= 1.666141 \times 10^{15} - 1.7011 \times 10^{12}i \text{ s}^{-1}, \end{aligned} \quad (29)$$

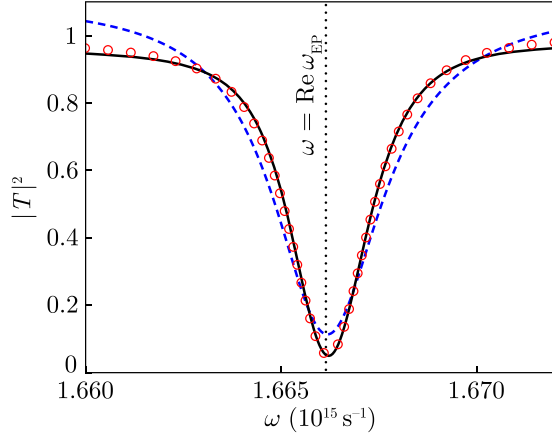


FIG. 3. TM-transmission spectra at the EP: rigorously calculated spectrum (circles), Fano line-shape approximation (dashed line), and second-order-pole approximation (17) (solid line).

where  $\omega_{\text{EP}} = \omega_{\text{p}}^{\text{TE}}(k_x^{\text{EP}}, k_y^{\text{EP}}) = \omega_{\text{p}}^{\text{TM}}(k_x^{\text{EP}}, k_y^{\text{EP}})$ . These values are the exact position of the EP, calculated using the rigorous coupled-wave analysis. Alternatively, the position of the EP can be estimated using Eqs. (14)–(16) and (27), which are based on the CMT. These equations give the following estimation of the EP parameters:

$$\begin{aligned} \tilde{k}_x &= 0.47494 \mu\text{m}^{-1}, \\ \tilde{k}_y &= 0.12783 \mu\text{m}^{-1}, \\ \omega_{\text{p}} &= 1.666139 \times 10^{15} - 1.6957 \times 10^{12}i \text{ s}^{-1}, \end{aligned} \quad (30)$$

which are close to the rigorously calculated parameters presented in Eq. (29). Therefore, the CMT with rigorously estimated parameters (27) predicts the position of the EP with

high accuracy. As an illustration, the exact  $(k_x^{\text{EP}}, k_y^{\text{EP}})$  and the approximate  $(\tilde{k}_x, \tilde{k}_y)$  positions of the EP are shown in Fig. 4(c) by the circle and point, respectively.

At the EP the line shape of the resonance is different from the conventional Fano and Lorentz line shapes [9,20]. Figure 3 shows the TM-transmission spectrum of the considered structure at  $k_x = k_x^{\text{EP}}$ ,  $k_y = k_y^{\text{EP}}$ . The circles show the rigorously calculated spectrum, while the approximation (17) is shown by the solid line. The parameters  $a$  and  $b$  of Eq. (17) were obtained by the numerical calculation of the residues of the transmission coefficient:

$$a = \text{Res}_{\omega=\omega_{\text{EP}}} T(\omega), \quad b = \text{Res}_{\omega=\omega_{\text{EP}}} (\omega - \omega_{\text{EP}})T(\omega). \quad (31)$$

The value of  $t_0$  was obtained by fitting the rigorously calculated complex transmission coefficient  $T(\omega)$  using the least-squares method. As a comparison, the dashed line in Fig. 3 shows the Fano approximation  $T = t_0 + a/(\omega - \omega_{\text{EP}})$ , where both  $t_0$  and  $a$  were obtained using the least-squares method. Figure 3 suggests that simple-pole Fano approximation does not describe resonance line shape at the EP, while Eq. (17) provides a good approximation of the transmission spectrum near the resonance frequency.

Another intrinsic feature of EPs is the permutation behavior of the modes complex frequencies when encircling an EP in the parameter space [31]. To illustrate this, we choose the contour in the  $k_x$ - $k_y$  space, as shown in Fig. 4(a). The contour starts at  $k_x = k_x^{\text{EP}}$ ,  $k_y = 0$ ; encircles the EP counterclockwise; and arrives to the starting point. At the starting point the structure supports two modes with frequencies  $\omega_{\text{TE}}$  and  $\omega_{\text{TM}}$ , which are the TE- and TM-polarized modes. The complex frequencies of these modes are shown by the black dots in Fig. 4(b). When changing the values of  $k_x$  and  $k_y$  in the described manner, the two modes move in the complex  $\omega$  plane, as shown in Fig. 4(b).

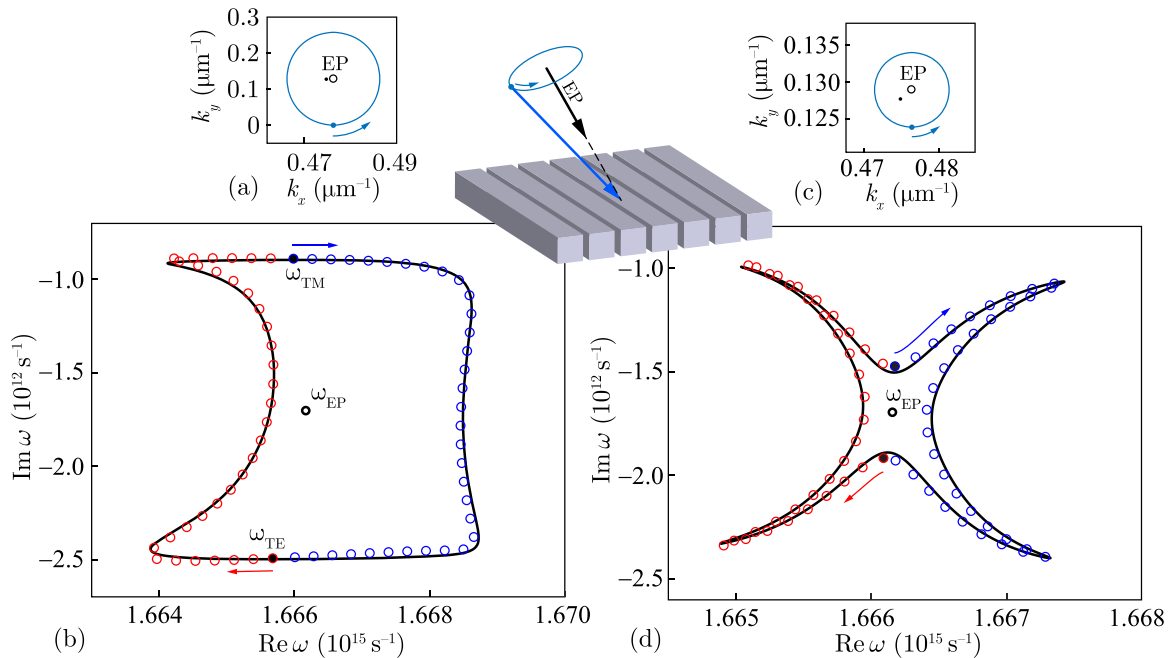


FIG. 4. Trajectories of the modes complex frequencies (b) and (d) when encircling EP in the  $k_x$ - $k_y$  space as shown in subfigures (a) and (c), respectively. Rigorously calculated trajectories are shown by circles, while the trajectories obtained using the CMT [Eqs. (11) and (12)] are shown by solid lines. Inset: Direction of the incident light when encircling the EP direction.

However, after encircling the EP in the parameter space once, the eigenfrequencies return not to their initial positions but interchange positions with each other. Similar behavior for a different contour in the  $k_x$ - $k_y$  space is shown in Figs. 4(c) and 4(d). Thus, we have shown that encircling the EP in the  $k_x$ - $k_y$  space results in eigenfrequencies permutation which is the evidence of an exceptional point [31].

The circles in Figs. 4(b) and 4(d) show the rigorously calculated complex frequencies trajectories, while the solid lines are obtained using the proposed analytical model [Eqs. (11) and (12)]. According to Fig. 4, the proposed model provides good agreement with the rigorous full-wave simulations.

## V. CONCLUSION

We have shown that in the case of conical mounting photonic crystal slabs exhibit cross-polarization mode coupling. This effect—coupling of the dispersion curves of quasi-TE and quasi-TM modes—has been described by means of the developed spatiotemporal coupled-mode theory. We have shown that by choosing the direction of incident light one can obtain an exceptional point due to coalescence of the two modes of the structure. The coupled-mode theory allowed us to obtain a simple analytical expression for the scattering

matrix, the transmission spectrum at the exceptional point, and the exceptional point condition. We have also obtained an approximate dispersion relation of the modes of the structure, which is in good agreement with the rigorous simulation results.

Further calculations show that even better agreement can be obtained if we assume that  $c_1^{\text{TE}}$  and  $c_1^{\text{TM}}$  in Eq. (7) depend on  $k_x$  and  $k_y$  [25]. In this case, by expanding  $c_1^{\text{TE}}$  and  $c_1^{\text{TM}}$  into a Taylor series up to  $k_x$  and  $k_y^2$  terms, we obtain the same Eq. (11) where  $\eta^{\text{TE}}$ ,  $\eta^{\text{TM}}$ ,  $v_g^{\text{TE}}$ , and  $v_g^{\text{TM}}$  are complex numbers.

Let us note that cross-polarization mode coupling discussed in this paper occurs due to breaking the reflection symmetry ( $xz$  symmetry plane) by introducing nonzero  $k_y$ . An alternative approach to breaking this symmetry is magnetization of the structure. Indeed, in Ref. [32] magnetization-induced cross-polarization mode coupling was demonstrated in longitudinally magnetized diffraction grating at  $k_y = 0$ . We believe the theory proposed in the current paper can be reformulated to describe the effects predicted in Ref. [32].

## ACKNOWLEDGMENT

This paper was funded by the Russian Science Foundation Grant No. 14-19-00796.

- 
- [1] A. Guo, G. J. Salamo, D. Duchesne, R. Morandotti, M. Volatier-Ravat, V. Aimez, G. A. Siviloglou, and D. N. Christodoulides, Observation of  $\mathcal{PT}$ -Symmetry Breaking in Complex Optical Potentials, *Phys. Rev. Lett.* **103**, 093902 (2009).
- [2] B. Zhen, C. W. Hsu, Y. Igarashi, L. Lu, I. Kaminer, A. Pick, S.-L. Chua, J. D. Joannopoulos, and M. Soljačić, Spawning rings of exceptional points out of dirac cones, *Nature (London)* **525**, 354 (2015).
- [3] P. Miao, Z. Zhang, J. Sun, W. Walasik, S. Longhi, N. M. Litchinitser, and L. Feng, Orbital angular momentum microlaser, *Science* **353**, 464 (2016).
- [4] J. Doppler, A. A. Mailybaev, J. Böhm, U. Kuhl, A. Girschik, F. Libisch, T. J. Milburn, N. Moiseyev, P. Rabl, and S. Rotter, Dynamically encircling an exceptional point for asymmetric mode switching, *Nature (London)* **537**, 76 (2016).
- [5] H. Hodaie, A. U. Hassan, S. Wittek, H. Garcia-Gracia, R. El-Ganainy, D. N. Christodoulides, and M. Khajavikhan, Enhanced sensitivity at higher-order exceptional points, *Nature (London)* **548**, 187 (2017).
- [6] W. Chen, Ş. K. Özdemir, G. Zhao, J. Wiersig, and L. Yang, Exceptional points enhance sensing in an optical microcavity, *Nature (London)* **548**, 192 (2017).
- [7] W. D. Heiss and A. L. Sannino, Avoided level crossing and exceptional points, *J. Phys. A* **23**, 1167 (1990).
- [8] W. D. Heiss, Repulsion of resonance states and exceptional points, *Phys. Rev. E* **61**, 929 (2000).
- [9] W. D. Heiss, The physics of exceptional points, *J. Phys. A* **45**, 444016 (2012).
- [10] W. D. Heiss and G. Wunner, A model of three coupled wave guides and third order exceptional points, *J. Phys. A* **49**, 495303 (2016).
- [11] J. Schnabel, H. Cartarius, J. Main, G. Wunner, and W. D. Heiss,  $\mathcal{PT}$ -symmetric waveguide system with evidence of a third-order exceptional point, *Phys. Rev. A* **95**, 053868 (2017).
- [12] V. Achilleos, G. Theocharis, O. Richoux, and V. Pagneux, Non-Hermitian acoustic metamaterials: Role of exceptional points in sound absorption, *Phys. Rev. B* **95**, 144303 (2017).
- [13] H. Cartarius, J. Main, and G. Wunner, Exceptional Points in Atomic Spectra, *Phys. Rev. Lett.* **99**, 173003 (2007).
- [14] H. Cartarius, J. Main, and G. Wunner, Exceptional points in the spectra of atoms in external fields, *Phys. Rev. A* **79**, 053408 (2009).
- [15] M. Kang, W. Zhu, H.-T. Wang, and M. Premaratne, Spawning a ring of exceptional points from a metamaterial, *Opt. Express* **25**, 18265 (2017).
- [16] H.-X. Cui, X.-W. Cao, M. Kang, T.-F. Li, M. Yang, T.-J. Guo, Q.-H. Guo, and J. Chen, Exceptional points in extraordinary optical transmission through dual subwavelength metallic gratings, *Opt. Express* **21**, 13368 (2013).
- [17] Y. Huang, G. Veronis, and C. Min, Unidirectional reflectionless propagation in plasmonic waveguide-cavity systems at exceptional points, *Opt. Express* **23**, 29882 (2015).
- [18] Q. Liu, B. Wang, S. Ke, H. Long, K. Wang, and P. Lu, Exceptional points in Fano-resonant graphene metamaterials, *Opt. Express* **25**, 7203 (2017).
- [19] Z. Lin, H. Ramezani, T. Eichelkraut, T. Kottos, H. Cao, and D. N. Christodoulides, Unidirectional Invisibility Induced by  $\mathcal{PT}$ -Symmetric Periodic Structures, *Phys. Rev. Lett.* **106**, 213901 (2011).
- [20] L. Schwarz, H. Cartarius, G. Wunner, W. D. Heiss, and J. Main, Fano resonances in scattering: An alternative perspective, *Eur. Phys. J. D* **69**, 196 (2015).

- [21] S. N. Ghosha and Y. D. Chong, Exceptional points and asymmetric mode conversion in quasi-guided dual-mode optical waveguides, *Sci. Rep.* **6**, 19837 (2016).
- [22] A. Pick, B. Zhen, O. D. Miller, C. W. Hsu, F. Hernandez, A. W. Rodriguez, M. Soljačić, and S. G. Johnson, General theory of spontaneous emission near exceptional points, *Opt. Express* **25**, 12325 (2017).
- [23] J. Wiersig, Sensors operating at exceptional points: General theory, *Phys. Rev. A* **93**, 033809 (2016).
- [24] D. A. Bykov and L. L. Doskolovich, Spatiotemporal coupled-mode theory of guided-mode resonant gratings, *Opt. Express* **23**, 19234 (2015).
- [25] D. A. Bykov, L. L. Doskolovich, and V. A. Soifer, Coupled-mode theory and Fano resonances in guided-mode resonant gratings: The conical diffraction mounting, *Opt. Express* **25**, 1151 (2017).
- [26] H. A. Haus, *Waves and Fields in Optoelectronics* (Prentice-Hall, Englewood Cliffs, NJ, 1984).
- [27] D. A. Bykov and L. L. Doskolovich, Numerical methods for calculating poles of the scattering matrix with applications in grating theory, *J. Lightw. Technol.* **31**, 793 (2013).
- [28] U. Günther, I. Rotter, and B. F. Samsonov, Projective Hilbert space structures at exceptional points, *J. Phys. A* **40**, 8815 (2007).
- [29] M. G. Moharam, E. B. Grann, D. A. Pommet, and T. K. Gaylord, Formulation for stable and efficient implementation of the rigorous coupled-wave analysis of binary gratings, *J. Opt. Soc. Am. A* **12**, 1068 (1995).
- [30] L. Li, Formulation and comparison of two recursive matrix algorithms for modeling layered diffraction gratings, *J. Opt. Soc. Am. A* **13**, 1024 (1996).
- [31] T. Kato, *Perturbation Theory for Linear Operators*, Die Grundlehren der Mathematischen Wissenschaften, Vol. 132 (Springer, Berlin, 1966).
- [32] D. A. Bykov and L. L. Doskolovich, Magneto-optical resonances in periodic dielectric structures magnetized in plane, *J. Mod. Opt.* **57**, 1611 (2010).